Journal of Inorganic Biochemistry 157 (2016) 80–93

Contents lists available at ScienceDirect

Journal of Inorganic Biochemistry

journal homepage: www.elsevier.com/locate/jinorgbio

Bovine serum albumin binding, antioxidant and anticancer properties of an oxidovanadium(IV) complex with luteolin

Luciana G. Naso [a], Luis Lezama [b,c], María Valcarcel [d], Clarisa Salado [d], Patricia Villacé [d], Danel Kortazar [d], Evelina G. Ferrer [a], Patricia A.M. Williams [a,*]

[a] Centro de Química Inorgánica (CEQUINOR, CONICET, UNLP), Departamento de Química, Facultad de Ciencias Exactas, Universidad Nacional de La Plata, 47 y 115-C.C.962-(B1900AVV), 1900 La Plata, Argentina
[b] Departamento de Química Inorgánica, Facultad de Ciencia y Tecnología, Universidad del País Vasco UPV/EHU, P.O. Box 644, 48080 Bilbao, Spain
[c] BCMaterials, Parque científico y Tecnológico de Bizkaia, Edificio 500-1, 48160 Derio, Spain
[d] Innoprot SL, Parque científico y Tecnológico de Bizkaia, Edificio 502-P1, 48160 Derio, Spain

ARTICLE INFO

Article history:
Received 14 October 2015
Received in revised form 16 January 2016
Accepted 18 January 2016
Available online 22 January 2016

Keywords:
Luteolin
Oxidovanadium(IV) complexes
Magnetic properties
Mechanisms of cytotoxic action
BSA binding

ABSTRACT

Chemotherapy using metal coordination compounds for cancer treatment is the work of the ongoing research. Continuing our research on the improvement of the anticancer activity of natural flavonoids by metal complexation, a coordination compound of the natural antioxidant flavone luteolin (lut) and the oxidovanadium(IV) cation has been synthesized and characterized. Using different physicochemical measurements some structural aspects of $[VO(lut)(H_2O)_2]Na\cdot 3H_2O$ (VOlut) were determined. The metal coordinated to two *cis*-deprotonated oxygen atoms (ArO^-) of the ligand and two H_2O molecules. Magnetic measurements in solid state indicated the presence of an effective exchange pathway between adjacent vanadium ions. VOlut improved the antioxidant capacity of luteolin only against hydroxyl radical. The antitumoral effects were evaluated on MDAMB231 breast cancer and A549 lung cancer cell lines. VOlut exhibited higher viability inhibition ($IC_{50} = 17\ \mu M$) than the ligand on MDAMB231 cells but they have the same behavior on A549 cells (*ca.* $IC_{50} = 60\ \mu M$). At least oxidative stress processes were active during cancer cell-killing. When metals chelated through the carbonyl group and one adjacent OH group of the flavonoid an effective improvement of the biological properties has been observed. In VOlut the different coordination may be the cause of the small improvement of some of the tested properties of the flavonoid. Luteolin and VOlut could be distributed and transported *in vivo*. Luteolin interacted in the microenvironment of the tryptophan group of the serum binding protein, BSA, by means of electrostatic forces and its complex bind the protein by H bonding and van der Waals interactions.

1. Introduction

Flavonoids are a broad class of low molecular weight phenolic compounds, plant secondary metabolites that are widely distributed in the leaves, seeds, bark and flowers of plants [1]. To date, more than 6000 flavonoids have been identified, although a much smaller number is important from a dietary point of view. Flavonoids consist of two benzene rings (A and B), which are connected by an oxygen containing pyrene ring (C) (Fig. 1). Those flavonoids that contain a hydroxyl group at C-3 position of the C ring are classified as 3-hydroxyflavonoids (flavonols, anthocyanidins, leucoanthocyanidins, and catechins), and those lacking this group are called 3-deoxyflavonoids (flavanones and flavones) [2].

Luteolin (3′,4′,5,7-tetrahydroxyflavone, lut) (Fig. 1), abundant in celery, green pepper, parsley, perilla leaf and chamomile tea beets, cabbage, cauliflower and olive oil, is one of the most common flavones [3].

The antioxidant properties of flavonoids are widely acknowledged. The two classical antioxidant structural features of flavonoids are the presence of a B-ring catechol group and a C2–C3 double bond and the presence of a free 3-OH group in conjugation with a cabonyl group at C4; the first serves to donate hydrogen/electron to stabilize a radical species and the second serves to bind transition metal ions such as iron and copper. Because luteolin and some of its glycosides fulfill these two structural requirements, it is not surprising that many luteolin-containing plants possess antioxidant properties [4].

Experimental data indicate that luteolin may prevent diabetes, cardiovascular and neurodegenerative diseases and shows anti-allergic activity *in vitro* and *in vivo* [4]. Also, potent anticancer effects have already been shown for luteolin in several studies. Luteolin inhibited the effects of tyrosine kinase involved in tumor cell proliferation and it is a possible uncompetitive inhibitor of N-acetyltransferase activity in human bladder cancer [5]. Moreover, this flavone inhibited the development of a series of solid tumors (colonic HT-29, HCT116, hepatic HepG2, SK-Hep-1, PLC/PRF/5, Hep3, cervical Hela, oral SCC-4) [6]. Shih et al. demonstrated that luteolin inhibited human breast cancer cell (MDAMB231)

* Corresponding author.
E-mail address: williams@quimica.unlp.edu.ar (P.A.M. Williams).

http://dx.doi.org/10.1016/j.jinorgbio.2016.01.021
0162-0134/

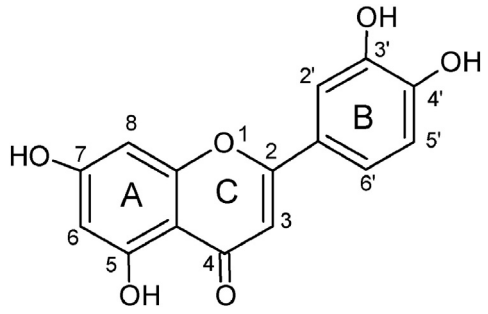

Fig. 1. Composition of luteolin and positioning of functional groups.

proliferation through inhibition of cell surface nicotine receptors [7] and on human leukemia cell lines (HL-60 cells) luteolin induced apoptosis by activation of the mitochondrial pathway [5]. Moreover, it was reported that luteolin and its structurally related flavonoid, apigenin, induced cell death on a variety of breast cancer cell lines (MDAMB231, SKBr3, MCF7, BT-474, and ZR75 cell lines) [8].

On the other hand, the success of cisplatin and its derivatives as anticancer agents has stimulated the development of metal-based compounds with flavonoids [9]. Oxidovanadium(IV) complexes with different flavonoids have been shown to have antioxidant and anticancer properties [10–18]. With the aim of ongoing the study of the relationship between the structure of the flavonoids and their oxidovanadium(IV) complexes with their activity, we have synthesized a VO(IV)–luteolin complex, $[VO(lut)(H_2O)_2]Na\cdot 3H_2O$ (VOlut), with a different composition than the earlier synthesized compound, $[VO(lut)_2]$ [19]. Structural information has been obtained using different physicochemical measurements both in solution and in solid state. Their antioxidant properties were analyzed *in vitro* and their anticancer effects on different cell lines have been evaluated. Mechanistic studies allow the determination that oxidative stress may be one of the causes of their deleterious effects on the breast MDAMB231 and lung A549 cancer cell lines. Their bovine serum albumin (BSA) binding properties have also been evaluated.

2. Materials and methods

2.1. Materials and measurements

Luteolin (Nanjing Zelang Medical Technology Co., Ltd.) and oxidovanadium(IV) chloride (50% aqueous solution, Carlo Erba) were used as supplied. Corning or Falcon provided tissue culture materials. Dulbecco's modified Eagle's medium (DMEM), and trypsin-ethylenediaminetetraacetic acid (EDTA) were purchased from Gibco (Gaithersburg, MD, USA), Tryple™ from Invitrogen (Argentina SRL) and fetal bovine serum (FBS) from GibcoBRL (Life Technologies, Germany). All other chemicals used were of analytical grade. Endotoxin-free Roswell Park Memorial Institute culture medium (RPMI) was purchased from Sigma-Aldrich (St Louis, MO).

Elemental analysis for carbon and hydrogen was performed using a Carlo Erba EA1108 analyzer. Vanadium content was determined by the tungstophosphovanadic method [20]. Thermogravimetric analysis was performed with Shimadzu systems (model TG-50), working in an oxygen flow of 50 $mL\cdot min^{-1}$ and at a heating rate of 10 $°C\cdot min^{-1}$. Sample quantities ranged between 10 and 20 mg. UV–vis spectra determinations were recorded with a Hewlett-Packard 8453 diode-array spectrophotometer. The diffuse reflectance spectrum was recorded with a Shimadzu UV-300 spectrophotometer, using MgO as a standard. Infrared spectra were measured with a Bruker IFS 66 FTIR spectrophotometer from 4000 to 400 cm^{-1} using the KBr pellet technique. A Bruker ESP300 spectrometer operating at the X-band and equipped with standard Oxford Instruments low-temperature devices (ESR900/ITC4) was used to record the spectrum of the complex at room temperature in the solid state. Anisotropic X band EPR spectra of frozen solutions were recorded at 150 K, after addition of 5% DMSO to ensure good glass formation. A computer simulation of the EPR spectra was performed using the program WINEPR SimFonia (version 1.25, Bruker Analytische Messtecnik, 1996). Magnetic susceptibility measurements on polycrystalline samples were performed in the temperature range of 5–300 K with a Quantum Design MPMS-7 superconducting quantum interference device magnetometer and using an applied field of 0.1 T. Diamagnetic corrections of the constituent atoms were estimated from Pascal's constants.

Fluorescence spectra were obtained using a Perkin Elmer (Beaconsfield, UK) LS-50B luminescence spectrometer equipped with a pulsed xenon lamp (half peak height less than 10 μs, 60 Hz), an R928 photomultiplier tube, and a computer working with FLWinlab.

2.2. Synthesis of $[VO(lut)(H_2O)_2]Na\cdot 3H_2O$ (VOlut)

Luteolin (1 mmol) was mixed with $VOCl_2$ (50% aqueous solution, 0.5 mmol) in absolute ethanol (20 mL). The pH value was adjusted to 5.0 by NaOH (1 M) addition. After refluxing for 3 h a dark green solid was obtained. The suspension was filtered off and the solid was washed three times with absolute ethanol and dried in an oven at 60 °C. Anal. calcd. for $C_{15}H_{17}O_{12}VNa$: C, 38.9; H, 3.6; V, 11,0. Na, 5.0. Exp.: C, 38.7; H, 3.7; V, 10.8; Na, 5.1%. UV–vis data for 1:1 $V(IV)O^{2+}$ to luteolin ratio, pH 5, λ_{max} (DMSO) 554 nm (ε, 176 $M^{-1}\cdot cm^{-1}$), >800 nm. Thermogravimetric analysis (TGA) (oxygen atmosphere, velocity, 50 mL min^{-1}): in a first step (71 °C) the three water hydration molecules are lost ($\Delta\Omega_{calc.}$ 11.7, $\Delta\Omega_{found}$ 11.6%). The two coordinated water molecules are lost at higher temperature (268 °C, $\Delta\Omega_{calc.}$ 7.8, $\Delta\Omega_{found}$ 7.7%) The final residue up to 900 °C was characterized by infrared spectroscopy as $NaVO_3$. The weight of the final residue was in agreement with the theoretical value (25.4%). Diffuse reflectance spectrum after deconvolution: 427 nm, 608 nm, and 796 nm.

2.3. Spectrophotometric titrations and stability studies

In order to establish the stoichiometry of the complex the molar ratio method was applied. A methanol–water solution (50% v/v) of luteolin (4×10^{-5} M) was prepared and its electronic spectrum recorded. The absorption spectra of different methanolic solutions (50%) of 4×10^{-5} M luteolin and $VOCl_2$ in ligand-to-metal molar ratios from 10 to 0.5 (pH 5.0, maintained by the addition of NaOH) were measured. Plots of the absorbance of each solution at 404 nm *vs.* the ligand-to-metal ratios allow the stoichiometric determinations. Stability studies have been performed measuring the variation of the VOlut electronic absorption spectra with time. The dissolution of the complex was performed in DMSO, under nitrogen atmosphere.

2.4. Antioxidant properties

2.4.1. Superoxide dismutase assay

The superoxide dismutase (SOD) activity was examined indirectly using the nitroblue tetrazolium (NBT) assay. The indirect determination of the activity of luteolin and the VOlut was assayed by their ability to inhibit the reduction of NBT by the superoxide anion generated by the phenazine methosulfate (PMS) and reduced nicotinamide adenine dinucleotide (NADH) system. As the reaction proceeded, the formazan color developed and a change from yellow to blue was observed which was associated with an increase of the intensity of the band at 560 nm in the absorption spectrum. The system contained 0.5 mL of sample, 0.5 mL of 1.40 mM NADH and 0.5 mL of 300 μM NBT, in 0.1 M KH_2PO_4–NaOH buffer (pH 7.5). After incubation at 25 °C for 15 min, the reaction was started by adding 0.5 mL of 120 μM PMS [21]. Then, the reaction mixture was incubated for 5 min. Each experiment was performed in triplicate and at least three independent experiments were performed in each case. The amount of luteolin or VOlut that

gave a 50% inhibition (IC_{50}) was obtained by plotting the percentage of inhibition *versus* the negative log of the concentration of the tested solution.

2.4.2. 1,1-Diphenyl-2-picrylhydrazyl assay

The antiradical activity of luteolin and VOlut was measured in triplicate using a modified method of Yamaguchi et al. [22]. A methanolic solution of 1,1-diphenyl-2-picrylhydrazyl radical ($DPPH^{\bullet}$) (4 mL, 40 ppm) was added to 1 mL of the antioxidant solutions in 0.1 M tris(hydroxymethyl)aminomethane–HCl buffer (pH 7.1) at 25 °C, giving a final concentration of 10 μM. After 60 min in the dark, the absorbance at 517 nm was measured and compared with the absorbance of the control prepared in a similar way without the addition of the antioxidants (this value was assigned arbitrarily as 100%).

2.4.3. Scavenging of the hydroxyl radical

Hydroxyl radicals were generated by the ascorbate–iron–H_2O_2 system. Briefly, the reaction mixture contained 3.75 mM 2-deoxyribose, 2.0 mM H_2O_2, 100 μM $FeCl_3$, and 100 μM EDTA without or with the tested compounds in 20 mM KH_2PO_4–KOH buffer, pH 7.4. The reaction was triggered by the addition of 100 μM ascorbate and the mixture was incubated at 37 °C for 30 min. Solutions of $FeCl_3$, ascorbate, and H_2O_2 were made up in deaerated water immediately before use. The extent of deoxyribose degradation by hydroxyl radical was measured with the thiobarbituric acid method [23,24].

2.4.4. Inhibition of peroxyl radical

Peroxyl radicals were generated by the thermal decomposition of 2,2-azobis (2-amidinopropane) dihydrochloride (AAPH) [24]. AAPH was chosen due to its ability to generate free radicals at a steady rate for extended periods of time (half life of 175 h). The consumption of pyranine was followed spectrophotometrically by the decrease in absorbance at 454 nm with a thermostated cell at 37 °C. The reaction solutions contained AAPH (50 mM), pyranine (50 μM) and several concentrations of the tested compounds. The delay of pyranine consumption (lag phase) was calculated as the time before the consumption of pyranine started (notable reductions in absorbance) [25].

2.5. Biological assays

2.5.1. Cell culture

A549 human lung cancer cell line was obtained from ABAC (Argentinean Cell Bank Association INEVH, Pergamino, Buenos Aires, Argentina). DMEM supplemented with 100 $U \cdot mL^{-1}$ penicillin, 100 $\mu g \cdot mL^{-1}$ streptomycin and 10% (v/v) fetal bovine serum was used as the culture medium. When 70–80% confluence was reached, cells were sub-cultured using TrypLE™ from Gibco (Gaithersburg, MD, USA), free phosphate buffered saline (PBS) (11 mM KH_2PO_4, 26 mM Na_2HPO_4, 115 mM NaCl, pH 7.4). MDAMD231 human breast cancer cell lines were obtained from HPA Culture Collection (Salisbury, United Kingdom). The cell line was cultured in endotoxin-free RPMI medium supplemented with 10% FBS, and 100 $U \cdot mL^{-1}$ penicillin and 100 $\mu g \cdot mL^{-1}$ streptomycin. Cultures were maintained at 37 °C in a humidified atmosphere with 5% CO_2 and passaged according to the manufacturer's instructions. For experiments, cells were grown in multi-well plates. When cells reached 70% confluence, the monolayers were washed twice with medium and then incubated with the different compounds.

2.5.2. Crystal violet assay

The compounds were dissolved in DMSO just before the experiment and a calculated amount of these solutions was added to the growth medium containing cells at a final DMSO concentration of 0.5% which had no discernible effect on cell-killing. The growth inhibitory effect towards the cancer A549 cell line was evaluated by means of the crystal violet bioassay. Briefly, 2.0×10^4 cells/well were seeded in 48-well microplates in growth medium (500 μL) and then incubated at 37 °C in a 5% carbon dioxide atmosphere. After 24 h, the medium was removed and replaced with a fresh one containing the compounds to be studied at the appropriate concentration. Triplicate cultures were established for each treatment. After 24 h, each well was stained with crystal violet and washed to remove the excess of dye. The crystal violet taken up by the cells was extracted with the buffer and the inhibition of cell growth induced by the tested compounds was detected by measuring the absorbance of each well at 540 nm. Mean absorbance for each drug dose was expressed as a percentage of the control untreated well absorbance and plotted *vs.* drug concentration.

Intracellular reactive oxygen species (ROS) generation in the A549 cell line was measured by oxidation of DHR to rhodamine. Cells were incubated during 30 min at 37 °C in 1.5 mL of PBS buffer alone (basal condition) or with the compounds in the presence of 10 mM DHR. Media were separated and the cell monolayers rinsed with PBS and lysated into 1 mL 0.1% Triton-X100. The cell extracts were then analyzed for the oxidized product rhodamine by fluorescence spectroscopy (excitation wavelength, 500 nm; emission wavelength, 536 nm), using a Perkin-Elmer LS 50B spectrofluorometer. Results were corrected for protein content, which was assessed by the method of Bradford [26].

In order to evaluate the morphology of the cells, they were grown in six well/plates and incubated overnight with fresh serum-free DMEM plus 0 (basal), 50 and 100 μM solutions of the complex. The monolayers were subsequently washed twice with PBS, fixed with methanol and stained with 1:10 dilution of Giemsa for 10 min. Next, they were washed with water and the morphological changes were examined by light microscopy.

2.5.3. MTT assay

Stock complex solutions were prepared by dissolving of compounds in DMSO with a manipulation time of 15 min. Breast cancer cells were seeded at a density of 5000 cells/well in 96 well plates, grown overnight and treated with either vehicle, luteolin, VOlut and oxidovanadium(IV) of different concentrations in FBS free medium. The dissolution vehicle, DMSO, yield a maximum final concentration of 0.5% in the treated well. After 24 h of incubation, 3-(4,5-methyl-thiazol-2-yl)-2,5diphenyl tetrazolium bromide (MTT) (Sigma-Aldrich, St. Louis, MO) was added at 100 μg/well for 2 h. The formazan products generated by cellular reduction of MTT were dissolved in DMSO and the optical density was measured at 560 nm using Sinergy 2 Multi Mode Microplater reader Biotek (Wisnooski, USA). All experiments were done in triplicate. Data were presented as proportional cell viability (%) by comparing the treated group with the untreated cells (control) in which the viability is assumed to be 100%.

For the high content analysis image assay the cancer cells were seeded at a density of 5000 cells/well in a collagen-coated 96 well plate and stained with fluorescent probes (Invitrogen, Life Technologies, Madrid, Spain) during 30 min: tetramethyl rhodamine methyl ester (TMRM) 50 μM for the measurement of mitochondrial depolarization related to cytosolic Ca^{2+} transients and 5-(and-6)-chloromethyl-2,7,dichlorodi hydrofluorescein diacetate acetyl ester (CMH2DCFDA) 1 μM for the determination of reactive oxygen species production (ROS). After 30 min cells were treated with 10 μM concentration of luteolin, VOlut and oxovanadium(IV) during 24 h. Some cells received 100 μM H_2O_2 as positive control for ROS and TMRM measurement. Image acquisition was performed using a Becton Dickinson Pathway plate imager with a 10× Olympus Objective. The excitation/emission filters for each probe were: 488/10 nm and 515 LP nm (ROS) and 555/28 nm and 647/78 nm (TMRM). Using specific AttoVision (BD) software algorithms, the mean intensity of each Region of Interest (ROI) was analyzed. Then cells were fixed with 3% of paraformaldehyde for 30 min at room temperature and permeabilized in 1% SDS for 10 min. Non-specific binding was blocked for 1 h with 4% BSA in PBS buffer and then the cells were incubated with 2 $\mu g \cdot mL^{-1}$ mouse monoclonal H2AX (Abcam, Cambridge, United Kingdom) for 1 h at room

temperature. Further wash steps removed unbound antibody prior to the addition of the secondary Alexa 633 goat anti-mouse antibody. Images of the number of cells with DNA damage were acquired on a BD Pathway™ Bioimager. Before the probes addition, conditioned medium from each well was collected for lactate dehydrogenase (LDH) assay. This assay was performed according to the manufacturer's protocol. LDH release to the culture medium was determined using a Sinergy 2 Multi Mode Microplater reader Biotek (Wisnooski, USA) at 340 nm. The results are expressed as the mean ± the standard error of the mean.

Mitotic arrest staining was determined by immunohistochemistry (IHC). Cells were fixed directly with 16% paraformaldehyde for a final concentration of 4% during 15 min. After the fixation step the samples were washed three times with PBS and permeabilized with PBS + 0.1% triton for 15 min. The samples were then blocked with PBS + bovine serum albumin (0.3%) for 15 min and finally anti-phospho-H3 polyclonal antibody (Life Technologies, Carlsbad, CA, USA) were added at 1/500 in PBS + 0.3% BSA for 60 min at room temperature. After three washing steps, 4′,6-diamidino-2-phenylindole (DAPI) and the secondary antibodies Alexa 488 (Life Technologies, Carlsbad, CA, USA) were added at 1/500 for 60 min to react against the primary antibody. The samples were then washed three times and measured in the Pathway 855 automated fluorescent microscope.

Statistical differences were analyzed using the analysis of variance method (ANOVA) followed by the test of least significant difference (Fisher).

2.6. Fluorescence quenching measurements

BSA was dissolved in Tris–HCl (0.1 M, pH 7.4) buffer to attain a final concentration of 6 μM. Luteolin, oxidovanadium(IV) cation and VOlut, were added dropwise to the BSA solution and left to rest to ensure the formation of homogeneous solutions with concentrations ranging from 2 to 100 μM. The fluorescence intensity was measured (excitation at 280 nm and emission at 348 nm) at 298, 303 and 310 K. For each sample and concentration, three independent replicates were performed. The measurements were carried out on a Perkin-Elmer LS-50B luminescence spectrometer (Beaconsfield, England) equipped with a pulsed xenon lamp (half peak height less than 10 μs, 60 Hz), an R928 photomultiplier tube and a computer working with FLWinLab software. Both excitation and emission slits were set at 10 nm throughout this study.

3. Results and discussion

3.1. Solid characterization of the complex

3.1.1. Vibrational spectroscopy

FT-IR spectrum data of luteolin and its oxidovanadium(IV) complex in KBr were compared in Table 1. The assignments were performed according to previous reports on flavonoids and luteolin [27–31] and by comparison with the previously investigated oxidovanadium(IV) flavonoid complexes [10,12]. In the region 4000–2400 cm^{-1} the broad band observed for luteolin is indicative of the H-bonding generated between the C═O and 5-OH group. Upon complexation and or deprotonation this pattern changes and the bands due to the phenolic group stretchings, ν(O–H), diminish their intensity.

The C═O stretching band at 1650 cm^{-1} remained unchanged upon complexation although its intensity was reduced, indicating that the carbonyl group was not involved in the complex formation. The bands assigned to C═C and C2═C3 and to C═C (ring C) stretchings appeared at the same wavenumbers for both the ligand and the complex and then, the interaction of the metal through the A and C rings of the ligand could be discarded. The interaction of VO(IV) with the 3′- and 4′-deprotonated OH groups of luteolin has been determined by the vibrational analysis of the FTIR spectra: a) the absorption band of luteolin at 1512 cm^{-1} (assigned to the stretching of the aromatic ring B) has been splitted into two components in VOlut and b) the band at 1309 cm^{-1} assigned to the C4′–OH stretching shifted to higher wavenumbers indicating an increase in the C–O bond order, which is normally observed when metal coordination involves the deprotonated *ortho*-phenolic (OH) groups on the B-ring of flavonoids [31]. The absorption peaks at 1258 cm^{-1} and 1168 cm^{-1} in luteolin are due to the combination of C–O and C–O–C stretching vibration modes and remained unchanged in the oxidovanadium(IV) complex, indicating that the etheric oxygen atom was excluded from involvement in the metal coordination. The V═O stretching vibration is observed as a shoulder of the weak vibrational band of the ligand at 947 cm^{-1}, and at relatively low frequencies (925 cm^{-1}), suggesting that the interaction of the V═O cation with the deprotonated OH-groups generates a resonance with ring B with a lengthening of the V═O bond. This wavelength value for the oxidovanadium(IV) ion is typical for mono- and disaccharide complexes with *cis*-deprotonated OH coordination [32,33]. This "monocatechol-like" coordination mode has previously been predicted for luteolin and determined for fisetin at pH values lower than 6.5 in a previous study on the coordination modes and geometry of oxidovanadium(IV) complexes with flavonoids in solution [34]. The following EPR studies concur with the FTIR determinations.

Table 1
Assignment of the main bands of the infrared spectra of luteolin and its oxidovanadium(IV) complex, VOlut (band positions in reciprocal centimeters).

luteolin	VOlut	Assignments
3387 br	3420 br	$\nu(O–H)_{water}$
3090 vs br	3194 s br, 3082 m br	$\nu(O–H)_{phenol}$
2970 br		ν(C–H)
2923 br	2924 sh	ν(C–H)
2862 br		ν(C–H)
2721 br		ν(C–H) see text
2632 br		ν(C–H)
2334 br		
1650 vs	1650 m	ν(C═O)
1618 vs	1623 vs	ν(C═O), ν(C2═C3), ring A quinoid str
1587 s	1576 s	ν(C═C), ring C
1512 vs	1515 sh	δ_{ip}(CH), ν(C═C)
	1486 m	
1444 m	1435 m	δ (7OH), δ_{ip} (C8H)
1369 vs		Ring A, C trigonal str, δ(5OH), δ(7OH), ν(C–OH)
1309 m	1353 m	νC4′–OH, νC3′–OH
1258 m	1260 ms	ν(C–O–C), ν(C–OH)
1168 m	1172 m	ν(C–OH) ν(C–O–C)
1125 m	1126 br	ν(C–O), δ (C–H arom)
1032 m	1038 m	δ_{ip}(CH)
997 sh		δ_{op}(CH)
947 w	947 w	
	925 sh	ν(V═O)

Relative intensities of the bands: vs: very strong, s: strong, m: medium, w: weak, sh: shoulder, br: broad.

3.1.2. Electron paramagnetic resonance (EPR) and magnetic behavior

The EPR spectra were obtained working with the microcrystalline powder in the temperature range from 298 K to 10 K. The spectrum of the complex at room temperature displays two signals (Fig. 2A), the typical of an isolated $V^{IV}O$ axial moiety and the other wider and weak. At lower temperatures it can be seen that the main envelope remained unchanged with the narrowing of the band but it also showed the disappearance of the wide signal. Thus, this absorption pattern should correspond to a compound with strong antiferromagnetic interactions. The main EPR signal shows the typical eight-line pattern spectrum for $V^{IV}O$ systems. The experimental spectrum has been simulated and the fitted spectrum showed good concordance with it (Fig. 2B).

The calculated spin Hamiltonian parameters were $g_{II} = 1.943$ and $g_{\perp} = 1.974$ and the hyperfine coupling constants were $A_{II} = 168 \times 10^{-4}$ cm^{-1} and $A_{\perp} = 65 \times 10^{-4}$ cm^{-1} ($g_{iso} = 1.963$, $A_{iso} = 99.33 \times 10^{-4}$ cm^{-1}). An empirical additivity relationship introduced by Chasteen [35] has frequently been used to determine the identity

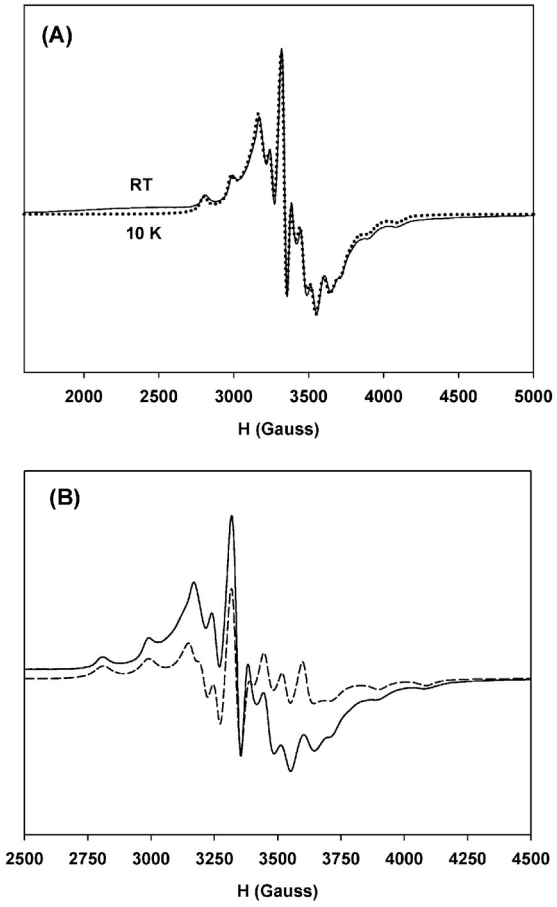

Fig. 2. (A) EPR polycrystalline spectrum (X-band, 9.399 GHz) at room temperature (RT) and 10 K. (B). Experimental (solid line, room temperature) and calculated (dotted dash line) EPR spectrum of the complex measured at X-band (9.495 GHz).

of the equatorial ligands in VO(IV) complexes: $A_z = \sum n_i A_{z,i}$ (n_i is the number of equatorial ligands of type i; $A_{z,i}$ is the contribution to the parallel hyperfine coupling from each of them). The parallel hyperfine coupling constant, A_{II}, was correlated with the number and types of ligands present in the equatorial coordination sphere. Each donor group has a specific contribution to this constant and the sum of the contributions of the four equatorial ligands can be used to argue for or against the presence of specific ligands. The calculated A_{II} value for the donor sets in a possible equatorial coordination in the complex was 168.6×10^{-4} cm^{-1} (two ArO^- and two H_2O molecules). This value was calculated considering the following literature data: ArO^- 38.6×10^{-4} cm^{-1} and H_2O 45.7×10^{-4} cm^{-1} [35], and agree with the experimental one, indicating that the binding mode of this complex could be expected to involve an equatorial coordination sphere with two oxygen atoms from two water molecules from the solvent and two *cis*-deprotonated oxygen atoms (ArO^- from ring B of the flavonoid moiety of the ligand) bound to the oxidovanadium(IV) center. The same coordination sphere has been determined for the complex formed with the flavonoid fisetin and the oxidovanadium(IV) cation in a DMSO/H_2O 50/50 v/v mixture solution, at pH 4.30, and it has been predicted an analogous complexing behavior for luteolin. Herein we have demonstrated that luteolin behaved in the same way than fisetin at the solid state when the preparative of the complex was performed at pH 5.5 in absolute ethanol [34].

The thermal evolutions of both the magnetic molar susceptibility (χ_m) and the $\chi_m T$ product ($\chi_m T = \mu_{eff}^2 / 8$) for $[VO(lut)(H_2O)_2]Na \cdot 3H_2O$ are shown in Fig. 3. At room temperature the value of $\chi_m T$ is equal to 0.26 $mL \cdot K \cdot mol^{-1}$, a value significantly lower than that expected for a system with non-interacting V(IV) ions (ca, 0.36 $mL \cdot K \cdot mol^{-1}$ using

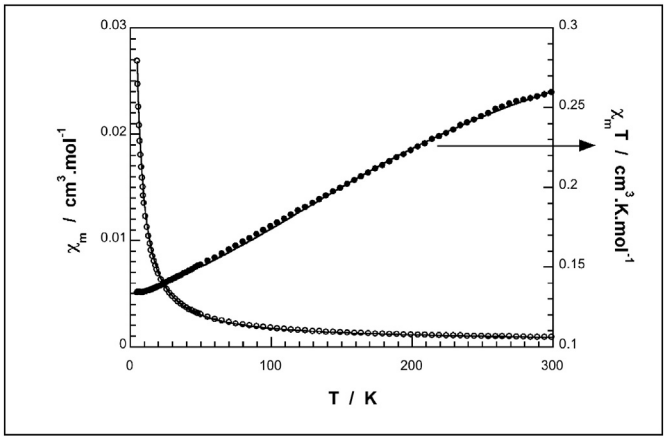

Fig. 3. Plots of χ_m and $\chi_m T$ for VOlut. The solid lines correspond to the best fit to Eq. (1).

the <g> = 1.963 value obtained from the EPR data). Upon cooling, $\chi_m T$ continuously decreases reaching a value of 0.14 $mL \cdot K \cdot mol^{-1}$ at 10 K and remains practically constant below that temperature. Moreover, the compound does not show a susceptibility maximum in the temperature range studied. These features are characteristics of a strong antiferromagnetic behavior combined with a paramagnetic contribution.

Despite the spin topology involved in the solid was unknown, we have tried to fit the magnetic data under different hypothesis: 1D, 2D and 3D regular systems of S = 1/2 and a dimeric option. Finally, the best results were obtained using the Heisenberg model with exchange interaction between pairs of vanadium ions with spins $\mathbf{S_i}$ and $\mathbf{S_j}$ of the form:

$$H = \sum_{i>j} H_{ij} = \sum_{i>j} -2J_{ij}\mathbf{S_i}\mathbf{S_j}$$

where we assume interactions between nearest neighbor vanadium ions on a chain (*i.e.*, $J_{ij} = J$ for $j = i \pm 1$ and $J_{ij} = 0$ otherwise).

The temperature dependence of the magnetic susceptibility for the $[VO(lut)(H_2O)_2]Na \cdot 3H_2O$ complex can satisfactorily be fitted to the empirical function introduced by Hall [36] to represent the numerical calculations performed by Bonner and Fisher [37] describing a uniformly spaced chain of spins with S = 1/2. An additional term which accounts for uncoupled VO(IV) ions following a simple Curie law and having the same *g* factor, was also included (Eq. (1)).

$$\chi = (1-\rho)\frac{Ng^2\beta}{kT}\left[\frac{A + Bx + Cx^2}{1 + Dx + Ex^2 + Fx^3}\right] + \rho\frac{Ng^2\beta^2}{4kT} \quad (1)$$

where $x = |J| / kT$, ρ is the percent of non-coupled ions, N and k are the Avogadro and Boltzmann constants, β is the Bohr magneton, A = 0.250, B = 0.14995, C = 0.30094, D = 1.9862, E = 0.68854 and F = 6.0626. The best-fit parameters obtained by minimizing the reliability factor $R = \Sigma[(\chi_m T)_{exp.} - (\chi_m T)_{cal}]^2 / \Sigma[(\chi_m T)_{exp}]^2$ are g = 1.97, J/k = −146.2 K, ρ = 0.36 and $R = 6.1 \times 10^{-4}$. As shown in Fig. 3, the calculated curves reproduce satisfactorily the experimental data in the whole investigated temperature range. The high value of the determined J parameter indicates that an effective exchange pathway is operative between adjacent vanadium ions in the compound. In summary, the final formula of the complex VOlut and the schema of the chains of adjacent V═O groups is depicted in Fig. 4.

3.2. Solution studies

3.2.1. Electronic UV–vis spectra

The flavonoids exhibit two major absorption bands in the UV–vis region: band I (usually 300–380 nm) corresponding to the B ring

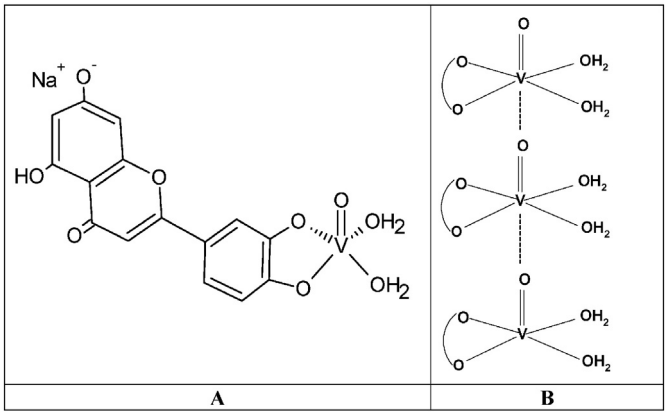

Fig. 4. A. Structural formula for the complex VOlut. B. Chains between adjacent VO groups.

(cynnamoyl system) and band II (usually 240–280 nm) corresponding to the A ring (benzoyl system, $\pi \rightarrow \pi^*$) [38]. The electronic spectra of luteolin were investigated as a function of pH in the methanol/water solutions (50% v/v) in the 2–12 pH range (Fig. S1). Based on the literature [39], the luteolin absorption spectra markedly shifted to the red by increasing the pH. Three acid–base dissociation steps have previously been determined for the ligand (pK_{a1}, 6.9; pK_{a2}, 8.6; pK_{a3}, 10.3). Our results showed that luteolin spectra remained unaltered from pH 2 to pH 8, with a maximum at 350 nm for band I. At higher pH values band I shifted to the red (405 nm) with two different patterns in the UV spectra at pH values 9–10 and 11–12 indicating the different deprotonations of the ligand. The first deprotonation (pK_{a1}) corresponding to the C7–OH moiety could not be observed by electronic spectroscopy. The other two deprotonations may be due to hydroxo groups at C4′–OH and C3′–OH or/and C5–OH, respectively [39].

The interaction of luteolin with oxidovanadium(IV) cation has been measured at different pH values in Fig. S2. The spectral bands showed a similar pattern than that of luteolin upon deprotonation. However, three regions of pH values were observed for the new band at 405 nm, that differ from those of the ligand: 2–4, 5–9, 10–12 but the positions of the bands by metal interaction remained similar to those of luteolin. It is known that the pK_a values of the Lewis bases diminished by the interaction with metal ions (Lewis acids). In the present case a bidentate complex formation and, subsequently, the 5-membered chelate ring with the metal ion facilitated the deprotonation of the hydroxo groups of ring B at lower pH values. Furthermore, the delocalization of the oxygen electrons of the deprotonated 3′,4′-dihydroxy group on ring B, assisted by the delocalization of the π electrons of the oxidovanadium(IV) ion led to the formation of a stable chelate formation with ring B [40].

The UV–vis spectra of luteolin and VOlut in methanol/water solution (50% v/v) are shown in Fig. 5. The electronic spectrum of luteolin at pH 5 was compared with the spectrum of the complex at the same pH value. When luteolin reacted with oxidovanadium(IV) cation the intensity of band II (256 nm, 268 nm(sh)) increased somehow. In contrast, band I (at 350 nm) began to decrease and the new band at 405 nm appeared at lower pH values than in luteolin. The formation of this new band is indicative of the metal coordination (the electronic pattern changed at a lower pH value) and of the interaction with ring B (the major changes are located at band II, and the unique formation of a chelate ring can be due through the cis-OH groups in 3′- and 4′-position).

To investigate the stoichiometry of the VOlut complex molar method was assayed and the experiments were conducted at pH 5. From Fig. 6 it can be seen that a 1:1 metal-to-ligand ratio has been determined. In a previous study a different solid complex of luteolin with oxidovanadium(IV) ion has been obtained and characterized [19]. According to the physicochemical determinations (FTIR, NMR and mass

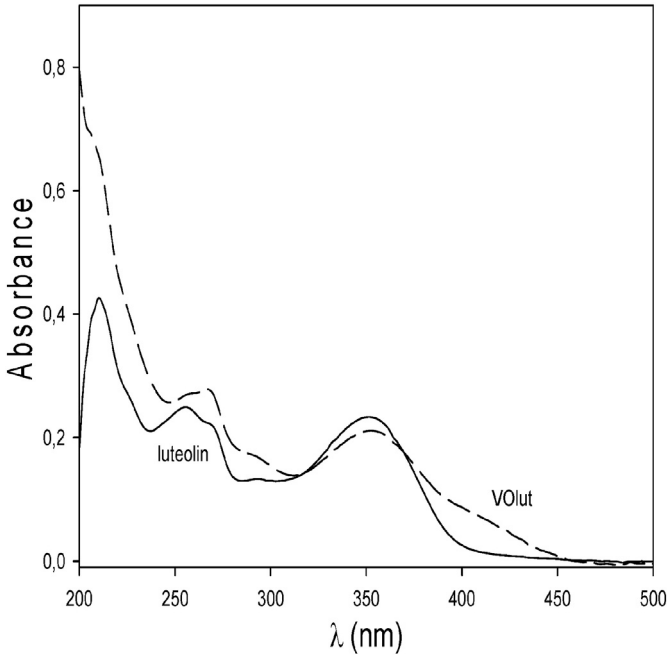

Fig. 5. UV–visible spectra of the ligand luteolin and the complex VOlut in methanol/water (50% v/v) solutions (pH = 5.0).

spectroscopies) and due to the different experimental conditions used in the preparative, the new solid consists in a $[VO(lut)_2]$ complex in which luteolin coordinates to the metal ion through C(4)O and the C(5)–O^- groups with a M:L 1:2 stoichiometry.

3.2.2. EPR spectroscopy

In order to assist in the identification of the solution species, the EPR spectrum of VOlut has been measured in frozen solution using DMSO as solvent (Fig. 7). Based on the calculated parameters, the experimental spectrum was simulated, and the fitted spectrum resulted in good concordance with the experimental one. The calculated spin Hamiltonian parameters were similar to those of the solid ($A_{II} = 169 \times 10^{-4}$ cm^{-1} and $A_{\perp} = 63.5 \times 10^{-4}$ cm^{-1} and $g_{II} = 1.945$ and $g_{\perp} = 1.979$). Another concern was the possible structure adopted by the pentacoordinated metal ion in solution (from a square pyramidal structure towards

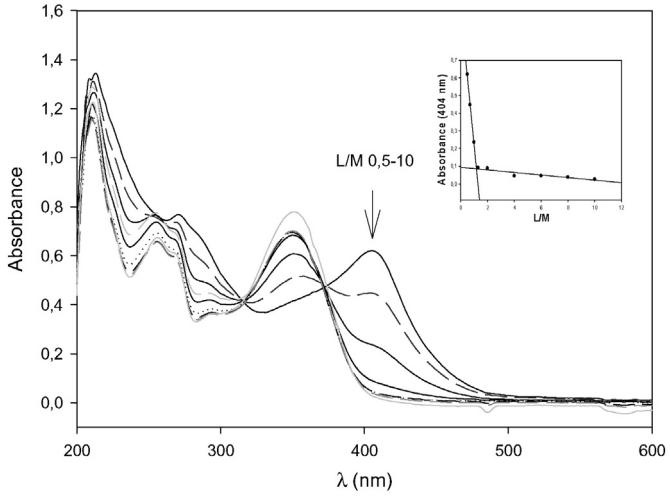

Fig. 6. UV–vis spectra of luteolin (4×10^{-5} M) and $VOCl_2$ in ligand-to-metal ratios (L/M) from 10.0 to 0.5 (pH 5.0). The arrow indicates increasing metal additions. Inset: spectrophotometric determination of the stoichiometry of the VOlut complex at 404 nm by the molar ratio method.

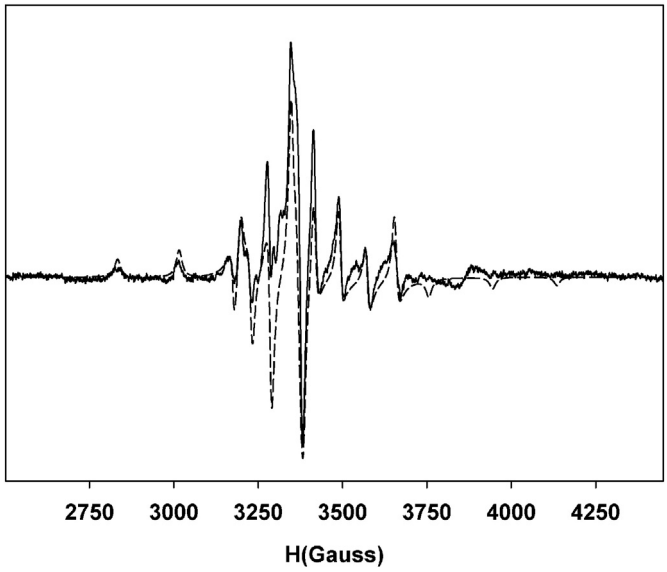

Fig. 7. Experimental (solid line) and calculated (short dash line) electron paramagnetic resonance (EPR) spectrum of a DMSO solution of VOlut (140 K, 3 mM) at X-band (9.49 GHz).

trigonal bipyramidal distortion). According to Cornman et al., EPR spectroscopy is susceptible to these structural changes, increasing the $|A_x - A_y|$ difference with the increase of the trigonal bipyramidal nature of the complex [41]. For square pyramidal complexes it is established that the V═O bond is along the z axis and the other four donor atoms are along the "x and y" axes, respectively. To this probable spatial distribution, an EPR spectrum without equatorial magnetic anisotropy would be expected, with $g_x = g_y$ and $A_x = A_y$ values [41]. The EPR spectrum of VOlut in frozen solution did not show relevant equatorial anisotropy and there was no splitting observed in the perpendicular high field signals suggesting that the oxidovanadium(IV) complex must adopt the square pyramidal geometry in solution, like in the solid state [41].

3.3. Antioxidant determinations

As stated above, the structure of luteolin (o-catechol in ring B and C2–C3 double bond) make the flavone a good antioxidant agent. Moreover, free radical scavenging ability of flavonoids is highly dependent of the presence of an OH moiety in C3, like quercetin, that increases the stability of the flavonoid radical and gave planarity to the flavonoid, thus allowing conjugation of rings B and C, and electron delocalization with stabilization of the phenoxy radical [1]. In this regard, luteolin does not behave as the better antioxidant flavonoid.

The measured antioxidant capacities of luteolin are shown in Table 2 and Fig. 8. Luteolin is not a good superoxide radical scavenger because it has a low superoxide dismutase (SOD) simil activity (considering our measured effect of the enzyme under the same conditions as 0.21 μM). Although a value of 58.5 μM has previously been reported [42], the positive control used in that study was not the native enzyme and then comparisons with our data cannot be performed. Comparing the SOD effect with that of the native enzyme should be taken into account when comparing the SOD catalytic activity of compounds. The medium DPPH$^\bullet$ sequestering power measured for luteolin is in concordance with previous results [43]. A medium antioxidant power against hydroxyl radicals has also been determined. Luteolin behaves as an excellent peroxyl scavenger and this data is in agreement with reported results [42]. Despite the disparity among methods of assessing activity, there is broad agreement on the substantial radical scavenging ability of luteolin.

Table 2
Free radical scavenging power of luteolin, the oxidovanadium(IV) complex (VOlut) and oxidovanadium(IV) cation. IC_{50}: half maximal inhibitory concentration.

	$O_2^{\bullet-}$ (IC_{50}, μM)	DPPH$^\bullet$ (IC_{50}, μM)	OH$^\bullet$ (IC_{50}, μM)	ROO$^\bullet$ (lag phase, min at 10 μM)
Luteolin	384	66.7 ± 10.2	50.7 ± 13.2	3.19
VOlut	417	>100	17.1 ± 5.2	2.15
$V(IV)O^{2+}$	15	>100	>100	1.23

The antioxidant power of luteolin has been compared with the effect of the oxidovanadium(IV) cation (that behaved as a good antioxidant agent against superoxide and peroxyl radicals) and VOlut complex (see Table 2 and Fig. 8). For the tested radicals luteolin behaved as a better antioxidant agent except against hydroxyl radical being VOlut a better scavenging agent. This behavior could be explained by the mode of coordination of the ligand to the metal ion. Because of the presence of dihydroxy groups in cis-position in ring B, the ligand coordinates to the metal through chelation with these groups as demonstrated by the physicochemical determinations (see above). Then, the complex formation precludes the involvement of 3′-OH and 4′-OH groups in the antioxidant action of the complex. Similar results have been obtained with a luteolin–Fe(III) complex [44].

3.4. Cell viability

First, the stability of VOlut complex has been studied. There was no observable variation in the electronic spectra of a DMSO solution of the complex at least during 30 min (*ca.* 2%, data not shown). These results demonstrated that during the manipulation time of the samples for the cellular determinations a significant amount of the complex is not decomposed.

Great efforts have focused on the rational design of metal-based anticancer agents that can be potentially used in cancer chemotherapy. Over the last four decades, a large number of metal complexes in addition to cisplatin have been extensively investigated and evaluated *in vitro* and *in vivo*, and some of them were at different stages of clinical studies. Among these complexes, platinum (Pt(II) and Pt(IV)), ruthenium (Ru(II) and Ru(III)), gold (Au(I) and Au(III), zinc (Zn(II)), La(III) and titanium (Ti(IV)) complexes were the most studied metal centers, though the action of the isolated cationic metals have not been compared in some of the studies [45–48]. In particular, some metal-complexes showed potent cytotoxic action on several breast cancer cells including the oxidovanadium(IV)–flavonoid complexes [16,17,49,50]. The effects of luteolin, VOlut and oxidovanadium(IV) cation on cell viability were examined in the breast cancer cell line MDAMB231 and the lung cancer cell line A549 (Fig. 9).

Cells were exposed to various concentrations (0–100 μM) of compounds for 24 h. Luteolin showed an IC_{50} = 88.3 μM towards the MDAMB231 cell line. These findings are in agreement with those of Lee et al. [51], Kim et al. (at concentrations lesser than 50 μM) [52] and Chen et al. [53] (who showed a 60% MDAMB231 cell viability at 70 μM of luteolin). VOlut displayed a strong deleterious effect with IC_{50} value of 17 μM for the MDAMB231 cell line. On the other hand, the cytotoxic behavior of the oxidovanadium(IV) cation occurred in a dose–response manner with higher IC_{50} values. It can be seen in Fig. 9 that the complexation improved the action of the ligand in the tested breast cancer cell line. On the contrary, a similar behavior has been found for luteolin and VOlut in the A549 cell lines (IC_{50} 66.3 and 60.5 μM, respectively) (Fig. 9) in agreement with the action found for their antioxidant activities. A lower value (3.1 μM) for the IC_{50} of luteolin in the A549 cell line has previously been found [54]. Notwithstanding, other reports gave different values which agree with that obtained in the present measurements [55,56].

The probable mechanism of the induction of cell death by the different compounds has been analyzed by high content assays for the MDAMB231 cell line and by measuring ROS generation and cellular morphology for the lung cancer cell line.

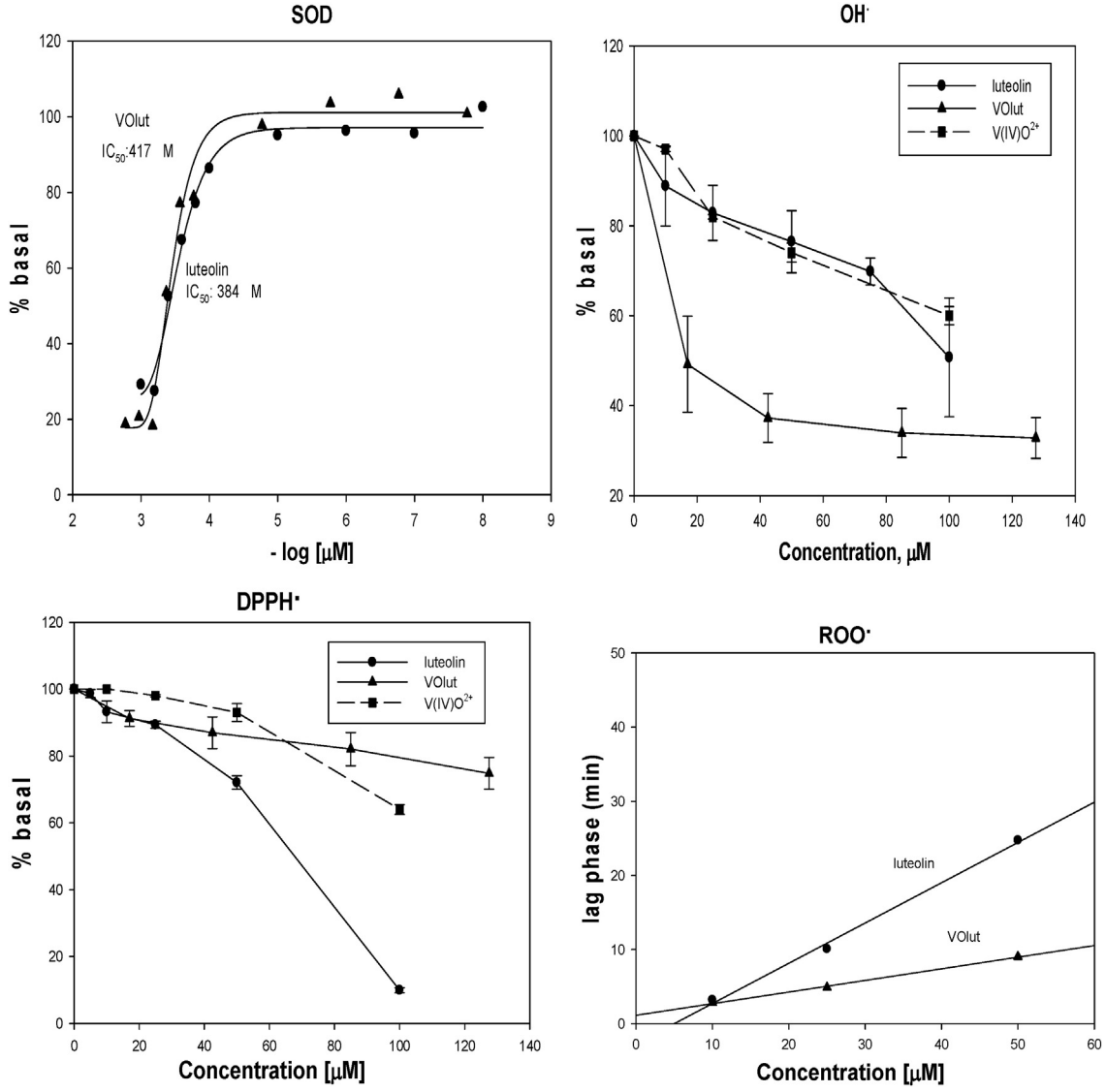

Fig. 8. Antioxidant behavior of luteolin, the oxidovanadium(IV) cation ($V(IV)O^{2+}$) and the complex VOlut. SOD: superoxide dismutase simil activity assay, $OH^{\bullet}$, hydroxyl radical, $DPPH^{\bullet}$, 1,1-diphenyl-2-picrylhydrazyl radical and $ROO^{\bullet}$, peroxyl radical.

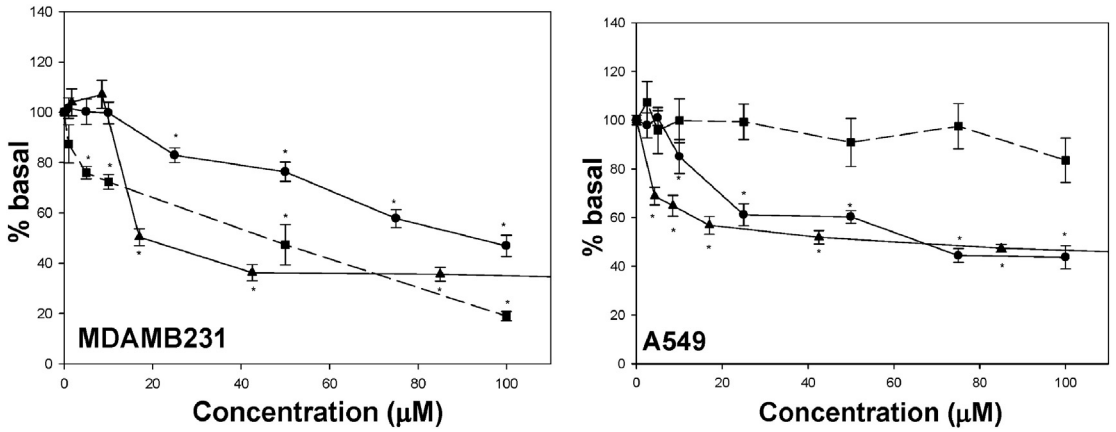

Fig. 9. Inhibitory effects of luteolin (circles), VOlut (triangles) and oxidovanadium(IV) cation (squares) on cell viability of MDAMB231 and A549 cell lines. All cell lines were treated with various concentrations of the compounds for 24 h. The results are expressed as the percentage of the basal level and represent the mean ± the standard error of the mean (SEM) from three separate experiments. Asterisks: significant values in comparison with the basal level ($P < 0.01$).

3.5. ROS production

Due to the particular antioxidant behavior of the complex because of its coordination mode, we have investigated whether cellular ROS level was also affected by both compounds. We measured ROS species in MDAMB231 cells with cell-permeable dye H2DFCDA, which is specifically cleaved to emit fluorescence in the presence of ROS [57], and by oxidation of DHR to rhodamine in the A549 cells (Fig. 10). Treatment with compounds at 10 μM and 60 μM for MDAMB231 and A549 cells, respectively (*ca.* VOlut IC_{50} values) for 24 h resulted in a significant elevation of intracellular ROS in both cellular types when compared to the basal rate. This increment was more important in MDAMB231 for the complex (6.5-fold higher) (Fig. 11) according to the high deleterious effects on cell survival (IC_{50} = 17 μM). On the contrary, oxidovanadium(IV) ion did not induce ROS production in both cell lines (Fig. 10 and Refs. [16, 17]). Thus the metal complexation of the flavonoid enhanced ROS production in the cancer cell lines according to its antioxidant behavior (poor superoxide scavenger and worst peroxyl scavenger than luteolin). The free-radicals mediated mechanism of toxicity has previously been found for others VOflavonoids on cell lines derived from rat osteosarcoma and breast and lung cancer [12,14,16,17].

Having identified from the first analysis that VOlut inhibitory effect was ROS dependent and selective for cancer cell lines, the most sensitive cell line MDAMB231 was selected for studying its probable mechanism of action. MDAMB231 cells were treated with VOlut, oxidovanadium(IV) cation and luteolin at 10 μM concentration and the results were summarized in Table 3 and the probable mechanism of the induction of cell death has been analyzed by high content assays (disruption of the mitochondrial membrane potential (TMRM), plasmatic membrane damage (LDH), nuclear membrane damage (H2AX), and mitotic arrest) and by measuring ROS generation and cellular morphology for the lung cancer cell line.

3.6. High content assay

3.6.1. Mitochondrial damage

Because mitochondria is considered as the main source of internal ROS in the cells, we further detected the changes of mitochondrial membrane potential (MMP) by TMRM dye in MDAMB231 cells treated with luteolin, oxidovanadium(IV) cation and VOlut [58]. TMRM probe is a cationic, lipophilic dye that accumulates in the negatively charged mitochondrial matrix in healthy cells with intact mitochondria. During the collapse of MMP, TMRM is dispersed throughout the cell and the fluorescence occurs with less intensity. The reduction in live cell population can therefore be quantified by the measurement of the decrease in TMRM fluorescence. The results revealed polarized normal cells in control cells, luteolin and oxidovanadium(IV)-treated cells whereas VOlut treatment showed population of depolarized cells >20% after 24 h of exposure. These results indicate that VOlut induces the loss of mitochondrial potential along with ROS generation in MDAMB231 cells.

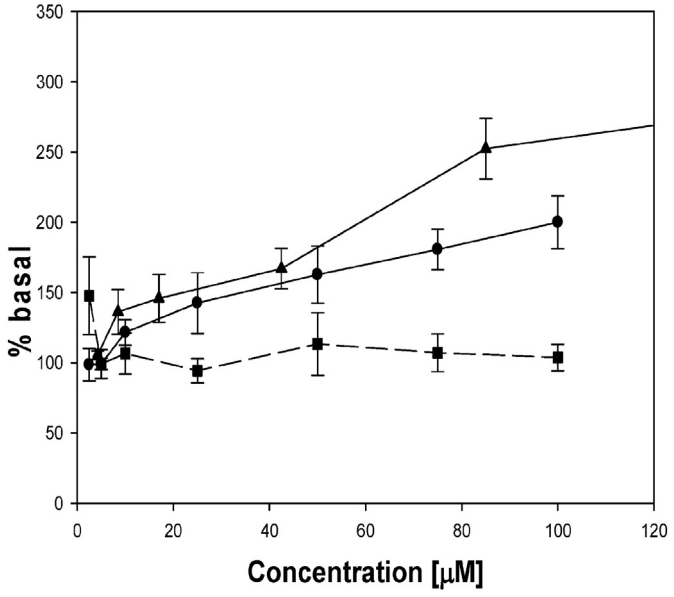

Fig. 10. Effects of ROS generation on A549 cell line for luteolin (circles), VOlut (triangles) and oxidovanadium(IV) (squares) cation. The results are expressed as the percentage of the basal level and represent the mean ± the standard error of the mean (SEM) from three separate experiments. Asterisks: significant values in comparison with the basal level ($P < 0.01$).

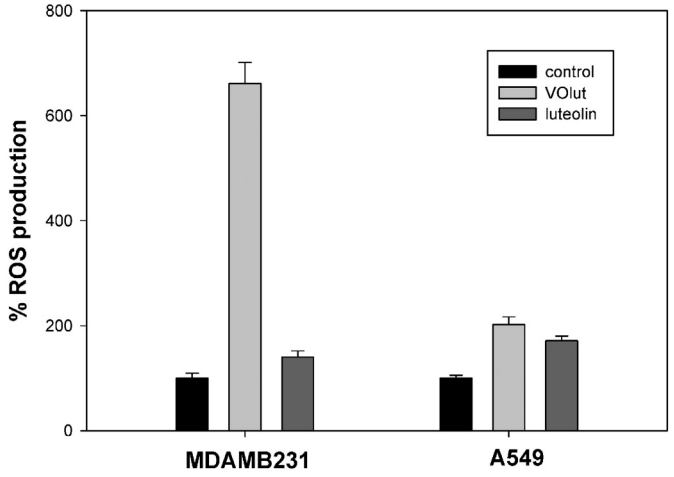

Fig. 11. Comparison of the percentage of ROS generation on MDAMB231 and A549 cell lines, for luteolin and VOlut at the IC_{50} concentration of the complex in each cell line. The results are expressed as the percentage of the basal level and represent the mean ± the standard error of the mean (SEM) from three separate experiments.

3.6.2. Induction of LDH release

LDH is a stable cytosolic enzyme that catalyzes the oxidation of L-lactate to pyruvate. Upon membrane damage in cells, this enzyme is released into the culture medium, suggesting the loss of membrane integrity [59]. Therefore, to confirm the cytotoxic effects of compounds on cancer cells, the presence of LDH in the culture medium was determined as another indicator of cytotoxicity. As shown in Table 3, similar levels of LDH were observed in the culture medium of luteolin-treated and untreated cells. However, treatment with VOlut significantly increased LDH released in the culture medium. A slight LDH increase in VO-treated cells was observed.

3.6.3. Nuclear damage

To test whether VOlut treatment resulted in nuclear damage, phosphorylated histone H2AX were determined by immunohistochemistry. This protein is a recognized marker for DNA damage. When DNA

Table 3
High content cytotoxicity assay. Effects of 10 μM luteolin, VOlut and oxovanadium(IV) cation at 24 h incubation on MDAMB231 cell line on ROS production, disruption of the mitochondrial membrane potential (TMRM), plasmatic membrane damage (LDH), nuclear membrane damage (H2AX), and mitotic arrest. Results are expressed as the percentage of the measured basal level and represent the mean values ± the standard error of the mean (SEM) from three separate experiments. Control: untreated cells.

	Control	VOlut	Luteolin	$V(IV)O^{2+}$
ROS	5.2 ± 0.4	34.4 ± 3.2	7.7 ± 0.9	5.1 ± 0.6
TMRM	100 ± 2.0	126 ± 1.1	117 ± 1.2	109 ± 5.5
LDH	100 ± 5.1	212 ± 3.3	96 ± 1.3	139 ± 8.3
H2AX	100 ± 4.7	175 ± 2.4	98 ± 2.1	141 ± 9.0
Mitotic arrest	8.2 ± 1.2	33.6 ± 2.1	23.1 ± 1.1	68 ± 8.0

damages, whether it is endogenous or exogenous, it forms double stranded breaks (DSBs), always followed by the phosphorylation of the histone, H2AX. H2AX is a variant of the H2A protein family, which is a component of the histone octomer in nucleosomes. DSBs can be induced by mechanisms such as ionizing radiation or cytotoxic agents [60]. From results on Table 3 it can be demonstrated that VOlut treated cells showed higher DNA damage (1.75 fold higher) compared to the basal state. Oxidovanadium(IV) cation exerted DNA damage in MDAMB231 in a lesser extent than the complex. However, no DNA damage was observed in luteolin-treated and cells. Thus the metal complexation of the flavonoid enhanced DNA damage in MDAMB231 cells.

3.6.4. Mitotic arrest

Cancer is often considered as a disease of cell cycle deregulation. Cell size, extracellular growth signals and DNA integrity are tightly regulated by multiple checkpoints in cell cycle progression. Cancer can originate from perturbation in the expression of positive of negative regulators of cell cycle machinery leading to abnormal proliferation of cancer cells. Thus, induction of cell cycle arrest in cancer cells is considered to be one of the crucial cancer treatments strategies. In order to evaluate the effect of VOlut on mitotic arrest, the PHH3 positive cells were determined by immunohistochemistry and then mitotic index (PHH3 positive nuclei/all nuclei) was calculated [61]. After 24 h of exposure to the compounds, the percentage of PHH3 positive cells was higher in VOlut and VO-treated cells than luteolin treated cells.

3.7. Morphological studies

Considering the cell-killing effect of VOlut in the A549 cell line we have determined that cell morphology varies according to the antiproliferative effect of the complex in a dose–response manner. It can be seen from Fig. 12 that at higher concentrations the number of viable cells diminished and morphologic alterations have been produced. An increment of cytoplasm condensation, presence of pycnotic nuclei and absence of nucleoli can be observed when VOlut concentrations were increased.

In conclusion, a deleterious effect of the complex on the breast and lung cancer cell lines has been observed. For both cell lines at least an oxidative stress mechanism has been proposed. We have also observed contradictory information on the effect of luteolin on these cell lines in the literature, although the comparisons of the data have been undertaken at the same incubation time. Moreover, the complex improved the cell-killing effects of the ligand on the breast cancer cells due to the DNA and plasmatic membrane damage, and to the improvement of the disruption of the mitochondrial membrane potential and mitotic arrest.

3.8. Structure–activity relationship

The antioxidant activities of the flavonoids in relation to their structure have widely been discussed [62]. Particularly, the presence of the C2C3 double bond and OH groups are essential for a good antioxidant behavior (see above), in special the presence of a 3-OH group allows planarity and electron delocalization with the concomitant increase of the stability of the phenyl radical of the flavonoid. As part of a project related to study the antioxidant and anticancer activities of structurally modified flavonoids we have selected the oxidovanadium(IV) cation to modify the structure by metal complexation.

Two main coordination types of metal coordination have been found: the chelation can involve C═O (carbonyl) with OH adjacent groups (quercetin, naringenin, chrysin, silibinin, morin), group I, or OH groups in cis- position on ring B or with a distant substituent of rings B or C (hesperidin, luteolin), group II. It has been observed that complexes of group I behave as better antioxidant agents than those of group II. The oxidovanadium(IV) complexes that have better antioxidant behavior were: VOsilibinin for superoxide radicals, VOchrysin for hydroxyl radicals, VOmorin for $DPPH^{\bullet}$ and VOnaringenin for $ABTS^{+\bullet}$. Altogether, the better antioxidant complex resulted to be VOsilibinin followed by VOmorin, both with an OH group at C3 position. In this point it has to be considered that we have not determined the VOquercetin antioxidant properties, though high antioxidant behavior against superoxide has been reported previously (IC_{50}, 0.63 μM) [63]. Although this value is three times lower than the value found for VOsilibinin, direct comparisons have not been performed because of the different methods used in both assays. In summary, we hypothesize that the π system of the V═O cation linked to C═O and OH in a chelated form allowed the resonance with rings A and C, giving rise to a probable stabilization of the phenyl radical generated by electron or H donation at C3 and/or C5 positions.

Both groups of VOflavonoid showed anticancer activities in the breast cancer cell line MDAMB231. VOsilibinin and VO chrysin, group I, displayed a high cytotoxic behavior (IC_{50}, 6 and 3 μM, respectively) improving the activity of the parent flavonoids (IC_{50}, 21 and 58 μM, respectively). Notwithstanding, an IC_{50} value of 17 μM has been found for luteolin (group II), similar to that of VOnaringenin (20 μM). Only the anticancer behavior of VOmorin is similar to that of the ligand (IC_{50} near 90 μM for both compounds). The structure–activity relationship, however, seems to be more difficult to analyze in the breast cancer cells because these complexes displayed different mechanisms of cell-killing inside the cells.

Moreover, the anticancer activity is highly dependent on the examined cell lines. For instance, in the osteosarcoma UMR106 cell line, VOchrysin, VOmorin and VOquercetin (group I) did not improve the action of the ligand, and VOsilibinin and VOhesperidin improved the antitumoral effect of the parent drug, being this effect higher for the latter complex. Furthermore, in the lung cancer cells A549, VOlut (IC_{50} *ca.* 60 μM) did not improve the action of the ligand and the IC_{50} value of VOnaringenin resulted higher than 100 μM. Once again, in the living cell lines, the different mechanisms that account for the cytotoxic effects of the VOflavonoid complexes make it difficult to make comparisons of their structures with their activities.

3.9. Interaction with bovine serum albumin (BSA)

Fluorescence quenching refers to any process, which decreases the fluorescence intensity of a sample. A variety of molecular interactions

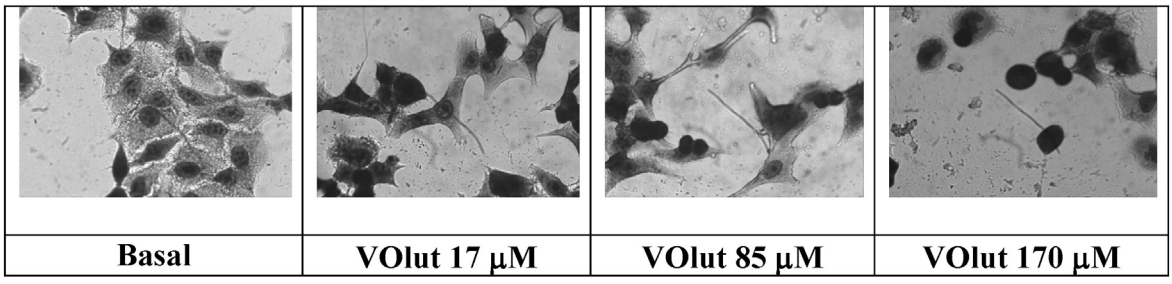

Fig. 12. Effects on cell morphology of the treatment of lung cancer cell lines with VOlut. Cells were incubated for 24 h without drug addition (basal) and with VOlut 17, 85 and 170 μM concentrations.

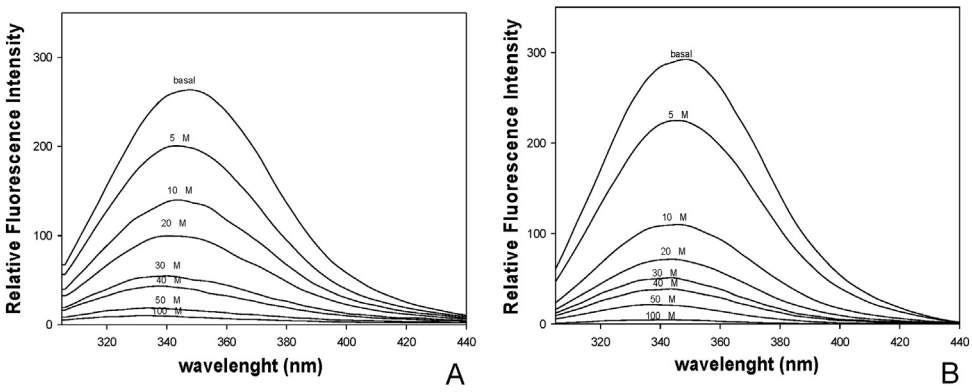

Fig. 13. The fluorescence spectra of BSA at various concentrations of luteolin (A) and VOlut (B). $\lambda_{ex} = 280$ nm, c(BSA) 6 μM, T = 298 K.

can result in quenching, including excited-state reactions, molecular rearrangements, energy transfer, ground-state complex formation and collisional quenching [64]. The interaction between luteolin and VOlut with BSA was investigated by evaluating the florescence intensity of the BSA before and after addition of these compounds. As it can be seen in Fig. 13, the intrinsic fluorescence of BSA resulted quenched in the presence of the compounds, indicating that there were some binding interactions between luteolin and VOlut with BSA. The maximum emission wavelength of BSA (λ_{max}) is located at 350 nm. As shown in Fig. 13, λ_{max} shifted to around 330 nm after the gradual addition of luteolin or VOlut. It is well known that the tryptophan (Trp) residue of BSA is mainly responsible for its intrinsic fluorescence and that the alterations in fluorescence emission spectra of BSA reflect the transformations that occurred nearby the microenvironment of the Trp residue. The addition of luteolin and VOlut induced a 20 nm blue shift on the emission peak, suggesting that the amino acid residue Trp was located in a more hydrophobic environment [65]. Besides, the blue shift implies that under simulated physiological conditions, the fluorescence data indicated that binding of luteolin to BSA is a combined quenching process where static quenching is prevailing [66].

Commonly, the fluorescence quenching can be described by the following Stern–Volmer equation:

$$F_0/F = 1 + K_{sv}[Q] = 1 + K_q\tau_0[Q] \quad (2)$$

where F_0 and F represent the fluorescence intensities before and after the addition of the quencher, respectively, K_q is the bimolecular quenching constant, τ_0 is the lifetime of the fluorophore in the absence of quencher, [Q] is the concentration of the quencher, and K_{SV} is the Stern–Volmer quenching constant (dynamic quenching constant). In order to confirm the quenching mechanism, the procedure of the fluorescence quenching was first assumed to be dynamic quenching. According to Eq. (2), the curve of F_0/F *versus* [Q] was plotted based on the experimental data (see Fig. 15). In many cases, the fluorophore can be quenched both by collision and by complex formation. When this is the case, the plot exhibits an upward curvature, concave towards the y-axis at high [Q], and F/F_0 is related to [Q] by the following modified form of the Stern–Volmer equation:

$$F_0/F = 1 + (K_D[Q])(1 + K_s[Q]) \quad (3)$$

where K_D and K_S are the dynamic and static quenching constants, respectively. This equation of second order with respect to [Q] accounts for the upward curvature observed at high [Q] when both static and dynamic quenching occur [67]. As shown in Fig. 14A and B, the deviation from linearity towards the y-axis at higher concentrations is an indication that both dynamic and static quenching processes have been involved in the mechanism of fluorescence of BSA with luteolin and VOlut.

A good linearity in the F_0/F *vs.* [Q] plots can be observed for luteolin and VOlut at lower concentrations (Fig. 14C and D and Table 4) and the K_q value resulted 3 orders of magnitude greater than the maximum diffusion collision quenching rate constant (2.0×10^{10} $M^{-1} \cdot s^{-1}$). This would indicate that the fluorescence quenching process of BSA may be mainly governed by a static quenching mechanism [17].

The binding constant (K_a) of the interaction of small molecules bounded to a set of equivalent sites on a macromolecule and the

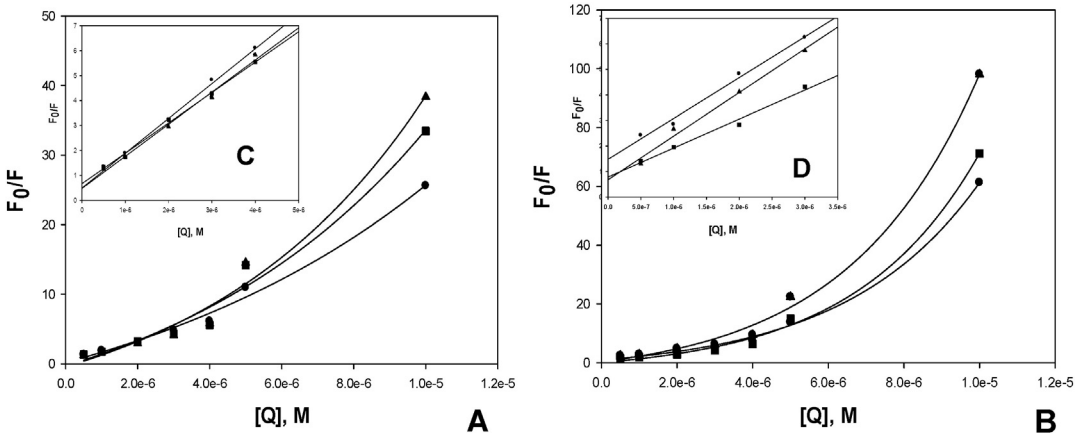

Fig. 14. Plots of F_0/F *vs.* [Q] for BSA with luteolin (A) and VOlut (B) at different temperatures ((●), 298 K; (▲), 303 K; (■), 310 K), $\lambda_{ex} = 280$ nm. Inset: F_0/F *vs.* [Q] of luteolin (C) and VOlut (D) ranging from 0.5×10^{-6} M to 4×10^{-6} M.

Table 4
Stern–Volmer constant (K_{sv}), quenching rate constant (K_q), binding constant (K_a) and n binding sites for the interaction of luteolin and VOlut with BSA (6 μM) in Tris–HCl buffer (0.1 M, pH 7.4).

Compounds	T (K)	K_{sv} ($\times 10^5$) (M^{-1})	r^2	K_q ($\times 10^{13}$) (M^{-1})	K_a ($\times 10^6$) (M^{-1})	n
Luteolin	298	13.97 ± 0.92	0.9926	13.97 ± 0.92	65.10 ± 0.90	1.48 ± 0.07
	303	12.88 ± 0.66	0.9917	12.88 ± 0.66	48.92 ± 0.87	1.31 ± 0.02
	310	12.19 ± 0.48	0.9962	12.19 ± 0.48	35.44 ± 0.52	1.27 ± 0.01
VOlut	298	17.09 ± 0.32	0.9876	17.09 ± 0.32	79.43 ± 0.56	1.29 ± 0.02
	303	16.01 ± 0.55	0.9899	16.01 ± 0.55	24.55 ± 0.72	1.21 ± 0.05
	310	11.36 ± 0.77	0.9853	11.36 ± 0.77	3.71 ± 0.21	1.07 ± 0.02

r^2 is the correlation coefficient for the K_{sv} values.

number of binding sites (n), can be calculated plotting log [(F_0 − F) / F] *versus* log [Q] (Eq. (4) and Fig. 15) [66]:

$$\log[(F_0 - F)/F] = \log K_a + n\log[Q]. \quad (4)$$

The value of K_a (Table 4) is significant to understand the distribution of the drug in plasma. A weak binding allows higher concentrations of drug in plasma, and then leads to a short lifetime or poor distribution of the drug, while a strong binding produces a decrease of concentrations in plasma improving the distribution and the pharmacological effect of the compound [68]. The number of binding sites (n = 1.07–1.48), of about 1.0, indicated that there exist one binding site of high affinity between luteolin and VOlut with BSA at different temperatures. Our results for n agree with those reported by Tang et al. but our measured K_a values resulted somehow higher [65]. These data showed that luteolin and VOlut could be distributed and transported *in vivo*.

In a previous study on the VOnaringenin system (VOnar) it was revealed that naringenin and its metal complex interacted with BSA producing a bathochromic shift (red shift) in the maximum emission wavelength of BSA suggesting that microenvironment of Trp residue turned to be more hydrophilic. On the contrary, the interaction of luteolin and VOlut complex with BSA produced a spectral blue shift which suggested an increase of the hydrophobicity of the region surrounding the tryptophan site [65]. The binding affinity of naringenin to BSA at 298 K ($K_a = 10.20 \times 10^4\ M^{-1}$) is smaller than that of luteolin ($K_a = 65.10 \times 10^6\ M^{-1}$), as expected. The hydroxylation on ring B and hydrogenation on ring C of flavonols significantly affected the binding/quenching process; in general, the hydroxylation increased the affinity and the hydrogenation decreased the affinity [69]. A C2C3 double bond favors near-planarity of rings B and C and molecules with near-planar structure easier enter the hydrophobic pockets in proteins [70]. This tendency is in concordance with the binding affinity observed for luteolin and VOlut (~$10^6\ M^{-1}$) in comparison with naringenin and VOnar (~$10^4\ M^{-1}$).

3.9.1. Thermodynamic parameters and nature of the binding forces

There are four types of intermolecular forces that could play a role in the interaction between compounds and BSA. These interactions can be described as *van der Waals* and electrostatic forces, hydrophobic interactions and hydrogen bond formation. The thermodynamic parameters of the binding reaction can be used for the determination of the type of interaction. The thermodynamic parameters luteolin and VOlut with BSA systems were calculated from the van't Hoff plots based on the temperature dependence of the binding constants. If the enthalpy change (ΔH) does not vary significantly in the temperature range studied, both ΔH and entropy change (ΔS) can be evaluated from the van't Hoff Eq. (5)

$$\ln K_a = -\Delta H/RT + \Delta S/R \quad (5)$$

where R is the gas constant, T is the experimental temperature, and K_a is the binding constant at corresponding T [71].

The free energy change (ΔG) is then estimated from the following equation:

$$\Delta G = \Delta H - T\Delta S. \quad (6)$$

Considering the negative free energy (ΔG) values obtained in these determinations, the spontaneity of all the binding processes can be demonstrated. It has been determined that for typical hydrophobic interactions, both ΔH and ΔS are positive, while negative enthalpy and entropy changes arise from van der Waals forces and hydrogen bonding formation in a low dielectric media. In addition, a specific electrostatic interaction between ionic species in an aqueous solution is characterized by a positive ΔS value and negative ΔH value [72]. The calculated values at 298 K for luteolin and VOlut were ΔH = −38.75 kJ/mol, ΔS = 19.45 J/mol and ΔG = −44.55 kJ/mol and ΔH = −196.93 kJ/mol, ΔS = −509.18 J/mol and ΔG = −45.19 kJ/mol, respectively. It can be concluded that luteolin interacted with BSA through electrostatic forces, probably as a result of the deprotonation of the ligand (pK_{a1}, 6.9) at the

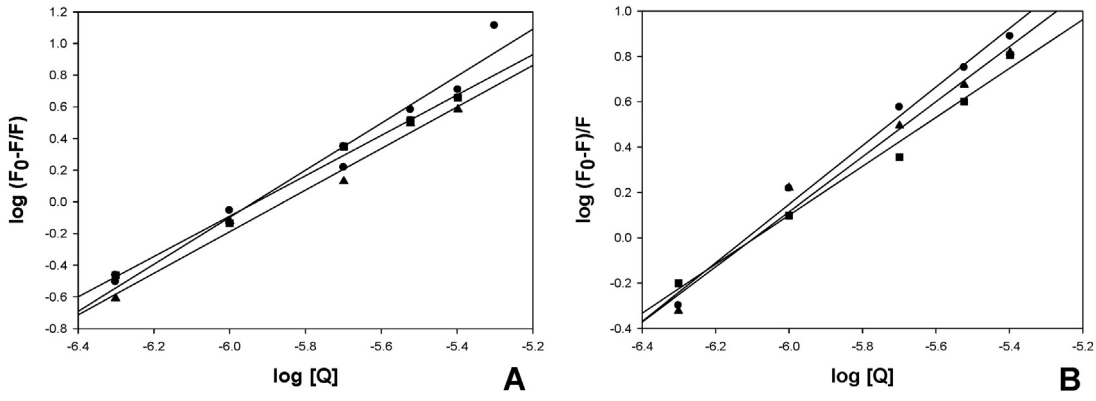

Fig. 15. Plots of log(F_0 − F)/F *vs.* log [Q] for the luteolin–BSA system (A) and VOlut-BSA system (B): (●) 298 K; (▲) 303 K; (■) 310 K, [BSA] = 6 μM, λ_{ex} = 280 nm.

pH value of the binding determinations, while for VOlut van der Waals forces and hydrogen bonds were operative.

It is worth mentioning that there are some discrepancies in the literature for the interaction of luteolin with albumin being the K_{sv}, K_a and the thermodynamic parameters quite different from each other. These differences could be attributed to the different experimental conditions used in each determination (albumin and flavonoid concentrations and different fractions of albumin) [65,66,73,74].

4. Conclusions

The results of this study indicated that the biological properties of flavonoid metal complexes are strongly dependent on the location and the number of coordinating or chelating sites. Flavonoids bind metals with different coordination modes: catecholate-like (O^-,O^-), acetylacetonate-like or maltol-like (CO,O^-) coordination. In particular, oxidovanadium(IV) cation used these different coordination modes when binding to flavonoids forming mono- or bi-chelated complexes. As a part of a project devoted to research the improvement of the anticancer and antioxidant capacities of flavonoids by structural modifications generated by metal complexation, a new oxidovanadium(IV)–luteolin complex have been synthesized. The interaction of the cis-OH groups with the metal (catecholate-like coordination) was determined by FTIR spectroscopy. By EPR and magnetic studies a coordination sphere with two water molecules and two ArO^- moieties was established and the presence of chains of adjacent VO groups was determined throughout the calculated effective exchange pathway. Because the CO and 5-OH groups of luteolin did not participate in metal binding, the antioxidant properties of luteolin and its metal complex did not strongly differ (contrary to the effect of coordination in the acetylacetonate-like or maltol-like modes) and similar anticancer effects in the lung cancer cell line A549 have been found for lutelin and VOlut with a probable oxidative stress mechanism responsible of the decrease of cell proliferation. A different behavior has been found in the breast cancer cell line MDAMB231, being the complex more cytotoxic. For this reason, a high content assay in the breast cell line was performed. In addition to cellular ROS generation and mitotic arrest of both luteolin and VOlut, the complex generates cytoplasmic and nuclear membrane damages. Binding of luteolin and VOlut to BSA is a combined quenching process while static quenching is prevailing. The thermodynamic parameters obtained from the Van't Hoff equation indicated that the processes were spontaneous and that electrostatic force was the predominant force in the luteolin-BSA complex and the interaction of VOlut with BSA occurred through H bonding and van der Waals interactions. Since a cytotoxic action of the luteolin and its complex was demonstrated, VOlut could be an interesting compound to be tested for cancer treatments in further *in vivo* studies.

Abbreviations

AAPH	2,2-azobis(2-amidinopropane) dihydrochloride
ABTS	2,2′-azinobis(3-ethylbenzothiazoline-6-sulfonic acid) diammonium salt
BSA	bovine serum albumin
Crystal violet	tris(4-(dimethylamino)phenyl)methylium chloride
DMEM	Dulbecco's modified Eagle's medium and
DPPH	1,1-diphenyl-2-picrylhydrazyl
EDTA	ethylenediaminetetraacetic acid
FBS	fetal bovine serum
H2AX	subtype of H2A histone
DCFH-DA	2′,7′-dichlorodihydrofluorescein diacetate
LDH	lactate dehydrogenase
Lut	luteolin
MMP	mitochondrial membrane potential
MTT	3-(4,5-dimethylthiazol-2-yl)-2,5diphenyltetrazolium bromide
NADH	reduced nicotinamide adenine dinucleotide
NBT	nitroblue tetrazolium
PMS	phenazine methosulfate
PBS	phosphate-buffered saline
PHH3	phosphohistone-H3
ROI	regions-of-interest
ROS	reactive oxygen species
RPMI medium	Roswell Park Memorial Institute culture medium
TMRM	tetramethyl rhodamine methyl ester
VOlut	$[VO(lut)(H_2O)_2]Na\cdot 3H_2O$

Acknowledgments

This work was supported by UNLP, CONICET, CICPBA (PICyT 813/13) and ANPCyT (PICT-2013-0569), Argentina. EGF and LGN are research fellows of CONICET. PAMW is a research fellow of CICPBA, Argentina. Convenio de vinculación tecnológica. Expte-CONICET-004200/13; TQ1/13.

Appendix A. Supplementary data

Supplementary data to this article can be found online at http://dx.doi.org/10.1016/j.jinorgbio.2016.01.021.

References

[1] K.E. Heim, A.R. Tagliaferro, D.J. Bobilya, J. Nutr. Biochem. 13 (2002) 572–584.
[2] I. Erlund, Nutr. Res. 24 (2004) 851–874.
[3] K. Xu, B. Liu, Y. Ma, J. Du, G. Li, H. Gao, Y. Zhang, Z. Ning, Molecules 14 (2009) 3486–3493.
[4] M. López-Lázaro, Mini Rev. Med. Chem. 9 (2009) 31–59.
[5] A.C. Cheng, T.C. Huang, C.S. Lai, M.H. Pan, Eur. J. Pharmacol. 509 (2005) 1–10.
[6] X. Cai, T. Ye, C. Liu, W. Lu, M. Lu, J. Zhang, M. Wang, P. Cao, Toxicol. in Vitro 25 (2011) 1385–1391.
[7] Y. Leun Shih, H.C. Liu, C.C.-S. Chen, C.-H. Hsu, M.-H. Pan, H.H.-W. Chang, C.C.-H.H. Chang, F.-C. Chen, C.-T. Ho, Y.-Y. Yang, Y.Y.-S.S. Ho, J. Agric. Food Chem. 58 (2010) 235–241.
[8] S. Yadegarynia, M. Bremer, J.B. White, Evaluation of flavonoids as agents to inhibit breast cancer, FASEB J. (2009) (Meeting Abstract Supplement, 712.6).
[9] M. Tan, J. Zhu, Y. Pan, Z. Chen, H. Liang, H. Liu, H. Wang, Bioinorg. Chem. Appl. 2009 (2009) 1–9.
[10] E.G. Ferrer, M.V. Salinas, M.J. Correa, L.G. Naso, D.A. Barrio, S.B. Etcheverry, L. Lezama, T. Rojo, P.A.M. Williams, J. Biol. Inorg. Chem. 11 (2006) 791–801.
[11] S.B. Etcheverry, E.G. Ferrer, L. Naso, J. Rivadeneira, V. Salinas, P.A.M. Williams, J. Biol. Inorg. Chem. 13 (2008) 435–447.
[12] L.G. Naso, E.G. Ferrer, L. Lezama, T. Rojo, S.B. Etcheverry, P.A.M. Williams, J. Biol. Inorg. Chem. 15 (2010) 889–902.
[13] E.G. Ferrer, P.A.M. Williams, Modification of flavonoid structure by oxovanadium(IV) complexation. Biological effects, in: K. Yamane, Y. Kato (Eds.), Handbook on Flavonoids: Dietary Sources, Properties and Health Benefits, Nova Science Publishers, Inc, New York 2011, pp. 145–190.
[14] L.G. Naso, E.G. Ferrer, N. Butenko, I. Cavaco, L. Lezama, T. Rojo, S.B. Etcheverry, P.A.M. Williams, J. Biol. Inorg. Chem. 16 (2011) 653–668.
[15] L. Naso, L. Lezama, T. Rojo, S.B. Etcheverry, M. Valcarcel, M. Roura, C. Salado, E. Ferrer, P.A.M. Williams, Chem. Biol. Interact. 206 (2013) 289–301.
[16] L.G. Naso, M. Valcarcel, P. Villacé, M.l. Roura-Ferrer, C. Salado, E.G. Ferrer, P.A.M. Williams, New J. Chem. 38 (2014) 2414–2421.
[17] M.S. Islas, L.G. Naso, L. Lezama, M. Valcarcel, C. Salado, M. Roura-Ferrer, E.G. Ferrer, P.A.M. Williams, J. Inorg. Biochem. 149 (2015) 12–24.
[18] I.E. León, V. Porro, A.L. Di Virgilio, L.G. Naso, P.A. Williams, M. Bollatí-Fogulin, S.B. Etcheverry, J. Biol. Inorg. Chem. 19 (2014) 59–74.
[19] S. Roy, S. Mallick, T. Chakraborty, N. Ghosh, A.K. Singh, S. Manna, S. Majumdar, Food Chem. 173 (2015) 1172–1178.
[20] M. Onishi, Photometric Determination of Traces of Metals, fourth ed., Part II, Wiley, New York, 1998.
[21] C.C. Kuo, M. Shih, Y. Kuo, W. Chiang, J. Agric. Food Chem. 49 (2001) 1564–1570.
[22] T. Yamaguchi, H. Takamura, T.C. Matoba, J. Terao, Biosci. Biotechnol. Biochem. 62 (1998) 1201–1204.
[23] B. Halliwell, J.M.C. Gutteridge, O. Aruoma, Anal. Biochem. 165 (1987) 215–219.
[24] W.Y. Huang, K. Majumder, J. Wu, Food Chem. 123 (2010) 635–641.
[25] C.D. Hapner, P. Deuster, Y. Chen, Chem. Biol. Interact. 186 (2010) 275–279.
[26] M. Bradford, Anal. Biochem. 72 (1976) 248–254.
[27] S. Đorđević, M. Cakić, S. Amr, Facta Univ. 1 (2001) 87–93.
[28] J. Patora, B. Klimek, Acta Pol. Pharm. Drug Res 59 (2002) 139–143.
[29] J. Sunil, M. Sanjith Nath, S. Raja, B. Vinatha, Sci. J. Pharm. 1 (2010) 1–4.
[30] J. Li, L. Wang, H. Bai, B. Yang, H. Yang, Med. Chem. Res. 20 (2011) 88–92.
[31] S.B. Bukhari, S. Memon, M. Mahroof-Tahir, M.I. Bhanger, Spectrochim. Acta A 71 (2009) 1901–1906.
[32] E.J. Baran, J. Coord. Chem. 54 (2001) 215–238.
[33] P.A.M. Williams, S.B. Etcheverry, E.J. Baran, Carbohydr. Res. 329 (2000) 41–47.
[34] D. Sanna, V. Ugone, G. Lubinu, G. Micera, E. Garribba, J. Inorg. Biochem. 140 (2014) 173–184.
[35] N.D. Chasteen, in: L.J. Berliner, J. Reuben (Eds.), Biological Magnetic Resonance, 3, Plenum, New York, 1981.

[36] J.W. Hall, PH.D. Thesis, North Caroline University, cited by: W. H. Hattfield, J. Appl. Phys. 52 (1981) (1985).
[37] J.C. Bonner, M.E. Fisher, Phys. Rev. B 135 (1964) A640.
[38] S.M. Boue, C.H. Carter-Wientjes, B.Y. Shih, T.E. Cleveland, J. Chromatogr. A 991 (2003) 61–68.
[39] G. Favaro, C. Clementi, A. Romani, V. Vickackaite, J. Fluoresc. 17 (2007) 707–714.
[40] S. Shi, Y. Zhang, X. Chen, M. Peng, J. Agric, Food Chem. 59 (2011) 10761–10769.
[41] C.R. Cornman, K.M. Geiser-Bush, S.P. Rowley, P.D. Boyle, Inorg. Chem. 36 (1997) 6401–6408.
[42] A. Gomes, E. Fernandes, A.M.S. Silva, C.M.M. Santos, D.C.G.A. Pinto, J.A.S. Cavaleiro, J.L.F.C. Lim, Bioorg. Med. Chem. 15 (2007) 6027–6036.
[43] R. Hirano, W. Sasamoto, A. Matsumoto, H. Itakura, O. Igarashi, K. Kondo, J. Nutr. Sci. Vitaminol. 47 (2001) 357–362.
[44] A.H. Yang, X.Y. Shi, X. Li, F.F. Li, Q.Q. Zhang, S.X. Jiang, J.Z. Cui, H.L. Gao, RSC Adv. 4 (2014) 25227–25233.
[45] N. Muhammad, Z. Guo, Curr. Opin. Chem. Biol. 19 (2014) 144–153.
[46] N.P.E. Barry, P.J. Sadler, Chem. Commun. 49 (2013) 5106–5131.
[47] Q. Wang, Y. Huang, J. Zhang, X. Yang, Bioinorg. Chem. Appl. 2014 (2014) 1–9.
[48] N. Andrades Ikeda, E.M. Novak, D.A. Maria, A.S.S. Velosa, R.M.S. Pereira, Chem. Biol. Interact. 5 (2015) 184–191.
[49] B. Biersack, A. Ahmad, F.H. Sarkar, R. Schobert, Curr. Med. Chem. 19 (2012) 3949–3956.
[50] Z. Afrasiabi, P. Stovall, K. Finley, A. Choudhury, C. Barnes, A. Ahmad, F. Sarkar, A. Vyas, S. Padhve, Spectrochim. Acta A Mol. Biomol. Spectrosc. 114 (2013) 114–119.
[51] E. Lee, S. Oh, M. Sung, Food Chem. Toxicol. 50 (2012) 4136–4143.
[52] M.J. Kim, J.S. Woo, C.H. Kwon, J.H. Kim, Y.K. Kim, K.H. Kim, Cell Biol. Int. 36 (2012) 339–344.
[53] V. Chen, R.E. Staub, S. Baggett, R. Chimmani, M. Tagliaferri, I. Cohen, E. Shtivelman, PLoS ONE 7 (2012) e30107.
[54] G. Seelinger, I. Merfort, U. Wölfle, C.M. Schempp, Molecules 13 (2008) 2628–2651.
[55] X. Cai, Y. Tingmei, C. Liu, W. Lu, M. Lu, J. Zhang, M. Wang, P. Cao, Toxicol. in Vitro 25 (2011) 1385–1391.
[56] J. Yan, Q. Wang, X. Zheng, H. Sun, Y. Zhou, D. Li, Y. Lin, X. Wang, Biochem. Biophys. Res. Commun. 417 (2012) 842–846.
[57] M.H. Zhao, Z.T. Jiang, T. Liu, R. Li, Sci. World J. 2014 (2014) 1–6.
[58] P.S. Rao, A. Satelli, M. Moridani, M. Jenkins, U.S. Rao, Int. J. Cancer 130 (2012) 2703–2714.
[59] K.M. Yoo, I.K. Hwang, B. Moo, J. Food Sci. 74 (2009) C419–C425.
[60] L.J. Kuo, L.X. Yang, In Vivo 22 (2008) 305–310.
[61] H. Goto, Y. Tomono, K. Ajiro, H.I. Kosako, M. Fujita, M. Sakurai, K. Okawa, A. Iwamatsu, T. Okigaki, T. Takahashi, M. Inagaki, J. Biol. Chem. 274 (1999) 25543–25549.
[62] R.N. Pellegrini, A. Proteggente, A. Pannal, M. Yang, C. Rice-Evans, Free Radic. Biol. Med. 26 (1999) 1231–1237.
[63] R. Shukla, V. Barve, S. Padhye, R. Bhonde, Biometals 19 (2006) 685–693.
[64] A. Varlan, M. Hillebrand, Molecules 15 (2010) 3905–3919.
[65] L. Tang, W. Jia, Spectrochim. Acta A Mol. Biomol. Spectrosc. 103 (2013) 114–119.
[66] Y. Yang, Q. Hua, Y. Fan, H. Shen, Spectrochim. Acta A Mol. Biomol. Spectrosc. 69 (2008) 432–436.
[67] X. Shi, X. Li, M. Gui, H. Zhou, R. Yang, H. Zhang, Y. Jin, J. Lumin. 130 (2010) 637–644.
[68] Y. Zhang, S. Shi, X. Sun, X. Xiong, M. Pengn, J. Inorg. Biochem. 105 (2011) 1529–1537.
[69] X. Liu, X. Chen, J. Xiao, J. Zhao, F. Jiao, X. Jiang, J. Sol. Chem. 39 (2010) 533–542.
[70] J. Shi, H. Cao, Braz. J. Pharmacogn. 21 (2011) 594–600.
[71] X. Liu, X. Chen, J. Zhao, X. Jiang, Spectrosc. Lett. 43 (2010) 155–162.
[72] E.H. Liu, L.W. Qi, P. Li, Molecules 15 (2010) 9092–9103.
[73] S. Shi, Y. Zhang, X. Chen, M. Peng, J. Agric, Food Chem. 59 (2011) 10761–10769.
[74] M. Poór, Y. Li, G. Matisz, L. Kiss, S.K. Máté, T. Kőszegi, J. Lumin. 145 (2014) 767–773.